

Dielectric effects in the self-assembly of binary colloidal aggregates

Kipton Barros and Erik Luijten*

Department of Materials Science & Engineering and Department of Engineering Sciences & Applied Mathematics,
Northwestern University, Evanston, Illinois 60208, U.S.A.

(Dated: March 19, 2013 — Final version June 5, 2014)

Electrostatic interactions play an important role in numerous self-assembly phenomena, including colloidal aggregation. Although colloids typically have a dielectric constant that differs from the surrounding solvent, the effective interactions that arise from inhomogeneous polarization charge distributions are generally neglected in theoretical and computational studies. We introduce an efficient technique to resolve polarization charges in dynamical dielectric geometries, and demonstrate that dielectric effects *qualitatively* alter the predicted self-assembled structures, with surprising colloidal strings arising from many-body effects.

PACS numbers: 77.84.Nh, 82.70.Dd, 61.20.Ja, 77.22.Ej

Colloids are ubiquitous in systems of physical, chemical, and biological interest. In suspension, dissociation of surface groups frequently causes these particles to carry an electrical charge, resulting in electrostatic interactions that play an important role in colloidal stability, aggregation, and self-assembly [1–3]. Far less is known about the effect of induced polarization charges. Although molecular dynamics (MD) and Monte Carlo simulations of charged colloids are now commonplace, they rarely take into account dielectric effects and instead treat the dielectric constant as spatially uniform. This is particularly striking in view of the large dielectric contrast between typical colloids and an aqueous solution (e.g., $\kappa \approx 2.5$ for polystyrene *vs.* $\kappa \approx 80$ for water at 293 K), which induces significant polarization charges at the colloidal surface. Densely packed and anisotropic arrangements of dielectric objects make this approximation even less justified. Thus, there is a pressing need to assess the role of dielectric effects in self-assembly phenomena.

Proper treatment of dielectric effects has been limited by computational complexity. Only the simplest dielectric geometries permit analytical solution. For an interacting system of dielectric spheres, a series expansion has been derived [4], but this still requires expensive numerical evaluation. A more general approach is to numerically solve the induced bound charge self-consistently over discretized dielectric interfaces [5–10]. This approach does not constrain the geometry, but has not yet been efficient enough to allow simulation of dynamical dielectric objects, such as mobile colloids. Indeed, existing work has largely treated the dielectric geometry as static, focusing on ion distributions in planar [11–13] or spherical [14, 15] geometries.

In this Letter, we address this situation by presenting the first study of a dielectric system with a *fully dynamic* geometry, exploring the effect of polarization charges that respond to and influence the motion of charged colloids. Using an optimized simulation method [16] we explicitly demonstrate that dielectric interactions can *qualitatively* alter self-assembly in a prototypical size-asymmetric bi-

nary mixture of charged colloids in solution. In particular, polarization charge that binds a colloid pair can also effect repulsive three-body interactions, giving rise to string-like colloidal chains.

To gain insight in the role of dielectric mismatch between colloidal particles and the surrounding solvent, we briefly review systems of linear dielectrics, starting from the electrostatic (free) energy [17],

$$U = \frac{1}{2} \int \rho_f(\mathbf{r})\psi(\mathbf{r}) d\mathbf{r}, \quad (1)$$

where $\rho_f(\mathbf{r})$ is the free charge density and the potential $\psi(\mathbf{r})$ is defined through Poisson's equation,

$$\nabla \cdot [\kappa(\mathbf{r})\nabla\psi(\mathbf{r})] = -\rho_f(\mathbf{r})/\varepsilon_0, \quad (2)$$

with $\kappa(\mathbf{r})$ the material-specific and spatially varying dielectric constant and ε_0 the vacuum permittivity. If we scale $\kappa \rightarrow \gamma\kappa$ and $\rho_f \rightarrow \alpha\rho_f$ ($\alpha, \gamma > 1$), the energy scales as $U \rightarrow (\alpha^2/\gamma)U$, so that the behavior of a system is invariant if $\gamma = \alpha^2$. Here, we are interested in dispersions of colloidal particles with $\kappa = \kappa_{\text{obj}}$ in a medium (solvent) with $\kappa = \kappa_{\text{m}}$. Such a system is mathematically equivalent to colloids with *reduced* dielectric constant $\tilde{\kappa} = \kappa_{\text{obj}}/\kappa_{\text{m}}$ and scaled free charge density $\tilde{\rho}_f = \rho_f/\sqrt{\kappa_{\text{m}}}$ dispersed in a nonpolarizable solvent. Thus, without loss of generality, we vary only $\tilde{\kappa}$ in our calculations. To illustrate the role of this reduced dielectric constant, we consider the electrostatic energy of a neutral sphere of dielectric constant κ_{obj} and radius R and a point charge q at a distance $d > 0$ from its surface [17],

$$U_{\text{sphere}} = \frac{q^2}{8\pi\varepsilon_0\kappa_{\text{m}}R} \sum_{n=0}^{\infty} \frac{(1-\tilde{\kappa})n}{(1+\tilde{\kappa})n+1} \frac{1}{(1+d/R)^{2(n+1)}}. \quad (3)$$

Depending on $\tilde{\kappa}$, U_{sphere} (Fig. 1) ranges from attractive to repulsive [18]. If $\tilde{\kappa} > 1$, the induced surface bound charge closest to the point charge has the opposite sign as the point charge, and the dielectric effects are attractive (bottom inset). Conversely, if $\tilde{\kappa} < 1$, the induced

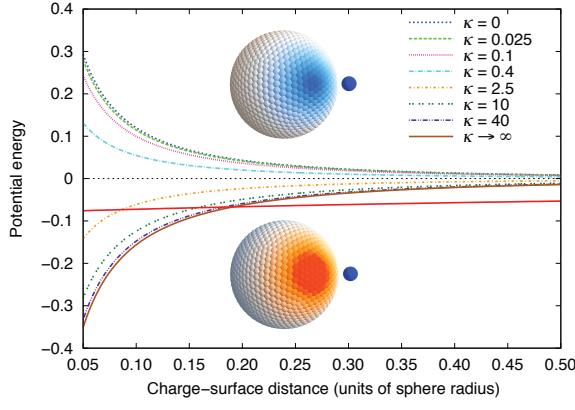


FIG. 1. Electrostatic energy (in units of $q^2/(\epsilon_0\kappa_m R)$) of a neutral sphere of radius R and dielectric constant κ_{obj} and a negative point charge q embedded in a medium of dielectric constant κ_m , as a function of ion-surface separation, for different values of the reduced dielectric constant $\tilde{\kappa} = \kappa_{\text{obj}}/\kappa_m$. The induced bound charges repel the point charge for $\tilde{\kappa} < 1$ (top inset; color coding represents calculated polarization charge density), whereas for $\tilde{\kappa} > 1$ the induced charges are attractive (bottom inset). The near-horizontal solid line indicates the pure Coulomb interaction for a reference system of two oppositely charged nondielectric spheres.

bound charge leads to repulsive dielectric effects (top inset). The two limits $\tilde{\kappa} = \{0, \infty\}$ correspond to a conducting solvent and a conducting sphere, respectively, but it is noteworthy that dielectric effects saturate well before either limit is reached. The asymmetry between $\tilde{\kappa} > 1$ and $\tilde{\kappa} < 1$ provides the starting point for exploring the effect of dielectric mismatch on colloidal aggregation. However, as we discuss below, physically rich behavior arises from the many-body interactions and the associated constraint that the net polarization charge on each colloid is fixed.

In our numerical treatment, we solve for the bound-charge density $\rho_b(\mathbf{r}) = -\nabla \cdot \mathbf{P}(\mathbf{r})$. Substitution of the polarization field $\mathbf{P}(\mathbf{r}) = \epsilon_0(\kappa(\mathbf{r}) - 1)\mathbf{E}(\mathbf{r})$ and the electric field $\mathbf{E}(\mathbf{r}) = -\nabla\psi(\mathbf{r})$ yields $\rho_b(\mathbf{r})/\epsilon_0 = \nabla \cdot [\kappa(\mathbf{r}) - 1]\nabla\psi(\mathbf{r})$. Comparison with Eq. (2) reproduces the well-known result

$$\nabla^2\psi(\mathbf{r}) = -[\rho_f(\mathbf{r}) + \rho_b(\mathbf{r})]/\epsilon_0. \quad (4)$$

We define \mathcal{G} to represent the inverse of the operator $-\nabla^2$. Its explicit action is $\mathcal{G}\rho(\mathbf{r}) = \frac{1}{4\pi} \int \frac{\rho(\mathbf{r}')}{|\mathbf{r}-\mathbf{r}'|} d\mathbf{r}'$. Equations (2) and (4) combined relate the free and bound charge,

$$\nabla \cdot [\kappa(\mathbf{r})\nabla\mathcal{G}(\rho_b(\mathbf{r}) + \rho_f(\mathbf{r}))] = -\rho_f(\mathbf{r}), \quad (5)$$

which can be rewritten as [19]

$$\mathcal{A}(\mathbf{r})\rho_b(\mathbf{r}) = b(\mathbf{r}), \quad (6)$$

where $\mathcal{A}(\mathbf{r})$ represents the linear operator

$$\mathcal{A}(\mathbf{r}) = -\nabla \cdot \kappa(\mathbf{r})\nabla\mathcal{G} = \kappa(\mathbf{r}) - (\nabla\kappa(\mathbf{r})) \cdot \nabla\mathcal{G} \quad (7)$$

$$b(\mathbf{r}) = (1 - \mathcal{A}(\mathbf{r}))\rho_f(\mathbf{r}). \quad (8)$$

Equation (6) will be solved for $\rho_b(\mathbf{r})$, from which the potential, $\psi(\mathbf{r}) = \mathcal{G}(\rho_f(\mathbf{r}) + \rho_b(\mathbf{r}))/\epsilon_0$, and other derived quantities follow. Equation (5) implies that the net charge in a compact region Ω with a uniform dielectric constant κ on its boundary is [16]

$$\int_{\Omega} [\rho_f(\mathbf{r}) + \rho_b(\mathbf{r})] d\mathbf{r} = \kappa^{-1} \int_{\Omega} \rho_f(\mathbf{r}) d\mathbf{r}. \quad (9)$$

As a consequence, the bound charge in regions of uniform κ is simply $\rho_b(\mathbf{r}) = (\kappa^{-1} - 1)\rho_f(\mathbf{r})$. The difficult (and generally ignored) task is to calculate $\rho_b(\mathbf{r})$ when $\nabla\kappa(\mathbf{r}) \neq 0$. We consider systems with sharp material interfaces, where the bound-charge density has to be calculated at the interface rather than in the entire volume—a considerable numerical simplification [7]. The strategy is to solve Eq. (6) as a discretized matrix equation for the surface charge density $\sigma(\mathbf{r})$ [8, 19],

$$\mathcal{A}_{ij}\sigma_j = b_i. \quad (10)$$

This matrix equation has the same mathematical content as previous discretizations [5–7].

However, in a *dynamical* situation, where dielectric objects move, \mathcal{A}_{ij} is evolving via its dependence on the dielectric geometry $\kappa(\mathbf{r})$. At each time step, the explicit construction of \mathcal{A}_{ij}^{-1} would require $\mathcal{O}(N^3)$ operations, where N is the number of discretized surface patches. Since this is prohibitively expensive, we instead opt to solve Eq. (10) for σ_j using an iterative method [8]. As shown in Ref. [16], iterative methods [20, 21] are desirable for two reasons: (i) explicit construction of the matrices \mathcal{A}_{ij} or \mathcal{A}_{ij}^{-1} is not required and the cost of each iteration scales as the cost of the matrix-vector product $\mathcal{A}_{ij}x_j$; (ii) convergence requires only a few iterations because the eigenvalues of \mathcal{A}_{ij} have a favorable structure. The only expensive, nonlocal piece of $\mathcal{A}_{ij}x_j$ (cf. Eq. (7)) is the calculation of $\nabla\mathcal{G}x$ —essentially finding $\mathbf{E}(\mathbf{r})$ for a given charge distribution $x(\mathbf{r})$. With an efficient Ewald solver one can numerically evaluate $\nabla\mathcal{G}x$ with $\mathcal{O}(N)$ [22] or $\mathcal{O}(N \ln N)$ [23] operations [9]. The number of iterations required to solve Eq. (10) at fixed numerical accuracy is bounded by $\log|\lambda_{\text{max}}/\lambda_{\text{min}}|$, the ratio of the largest and smallest eigenvalues of \mathcal{A}_{ij} . Since \mathcal{A}_{ij} , although neither symmetric nor normal, is diagonalizable with positive real eigenvalues that are bound by the extremal dielectric constants that occur in the system, $\kappa_{\text{min}} \leq \lambda \leq \kappa_{\text{max}}$ [16], the number of iterations scales at most as $\log[\kappa_{\text{max}}/\kappa_{\text{min}}]$, where typically $\kappa_{\text{max}}/\kappa_{\text{min}} \lesssim 25$. Furthermore, the worst-case convergence rates occur only in geometries with extreme aspect ratios, such as the infinite dielectric slab or cylinder. Employing GMRES, which requires only one matrix-vector product ($\mathcal{A}x$) per iteration and minimizes the residual in each iteration, we typically reach convergence (10^{-4} relative error in the electrostatic energy) within five iterations for a system of spherical objects—achieving a far

higher efficiency than prior approaches. For comparison, the iterative methods in Ref. [5–7, 9] essentially reduce to Richardson iteration, which converges more slowly and requires manual tuning of a relaxation parameter; if this parameter is not properly chosen, the method may even diverge. To make progress in simulating mobile dielectric objects, several additional steps are needed to ensure efficiency and accuracy. In each iteration we constrain the net charge on each object to its correct value via Eq. (9), thus eliminating a slow relaxation mode of the iterative solver and simultaneously improving the precision of the polarization charges. Furthermore, we replace the internal (free) charge q inside each object with a distribution of the charge q/κ_m that generates the same potential outside the object.

Lastly, in this first numerical study of mobile dielectrics we must address the electrostatic *force on a dielectric object*. This includes forces between induced and free charges as well as forces between polarization charges induced on different objects, and the resulting torques that may arise. A calculation of this force from first principles requires taking the derivative of the energy Eq. (1) with respect to object position [16]. If the free charge is rigidly fixed to the dielectric object this yields

$$\mathbf{F} = -\nabla U = \kappa_m \int_{\Omega} \mathbf{E}(\mathbf{r})(\rho_f(\mathbf{r}) + \rho_b(\mathbf{r})) d\mathbf{r}, \quad (11)$$

where Ω extends over the object. If the dielectric constant of the object matches the solvent, the integrand reduces to the electric component of the Lorentz force density, $\mathbf{f}(\mathbf{r}) = \kappa_m \mathbf{E}(\mathbf{r})(\rho_f(\mathbf{r}) + \rho_b(\mathbf{r})) = \mathbf{E}(\mathbf{r})\rho_f(\mathbf{r})$. A simple physical argument supporting Eq. (11) follows from the principle of effective moments [24, 25] where one replaces the dielectric object with a virtual distribution of free charge $\rho_v(\mathbf{r})$ that preserves the potential $\psi(\mathbf{r})$ external to the domain Ω of the object. A correct choice is indeed $\rho_v(\mathbf{r}) = \kappa_m(\rho_f(\mathbf{r}) + \rho_b(\mathbf{r}))$. The torque follows naturally from the force density.

The strategy outlined here now allows us to investigate a prototypical system of electrostatic self-assembly, namely a size-asymmetric binary mixture of charged spherical colloids. Such suspensions occur in a variety of contexts [3, 26–28]. It is important to note that we choose this salt-free model system to highlight dielectric effects. Experimental realizations generally contain salt, which screens the electrostatic interactions and thereby diminishes the role of polarization. We also disregard van der Waals interactions, notably Debye induction interactions (of similar origin as the induced interactions considered here, but far weaker [18]) and London dispersion forces (which display many-body effects as well [29, 30]). Our model constrains the colloids to have constant charge. In reality, charge regulation, in which the colloidal surfaces have a dynamic ionization state, provides a more accurate description than either constant-charge or constant-

potential boundary conditions [31–33], but its incorporation in a many-particle simulation would extend the computational complexity even further; furthermore, the present model offers the advantage of isolating the dielectric effects, permitting a *quantitative* assessment of their relevance compared to the nonpolarizable models widely employed in colloidal self-assembly.

The solvent (dielectric constant κ_m) contains an equal mixture of small colloids (diameter σ_{LJ} , free charge $-q$, dielectric constant κ_{small}) and large colloids (diameter $7\sigma_{LJ}$, $+q$, κ_{large}). The bound charge on the small colloids is distributed uniformly, and its fluctuations are assumed to be small. Indeed, we have verified that full treatment of these fluctuations would lead to corrections $\lesssim 1\%$ in the pair energy and $\sim 5\%$ in the pairwise forces [16]. For a large–small pair at separation $r \gg R = 3.5\sigma_{LJ}$, the induced interactions decay as r^{-4} , much faster than the direct Coulombic interactions. However, as Fig. 1 shows, at small separations $r \approx R$ dielectric interactions become important, reaching a magnitude comparable to the Coulombic interactions at contact ($d = 0.5\sigma_{LJ}/3.5\sigma_{LJ} \approx 0.14$) for $\tilde{\kappa} \gg 1$ or $\tilde{\kappa} \ll 1$.

To investigate the properties of this system, we perform large-scale MD simulations of mixtures containing 100 large colloids and 100 small colloids. The excluded-volume interactions between colloids are modeled via a purely repulsive shifted-truncated Lennard-Jones potential, $4\epsilon_{LJ}[(\frac{\sigma_{LJ}}{r-\delta})^{12} - (\frac{\sigma_{LJ}}{r-\delta})^6 + \frac{1}{4}]$ for $r \leq 2^{1/6}\sigma_{LJ} + \delta$ with $\delta = 0, 3\sigma_{LJ}$, or $6\sigma_{LJ}$ for small–small, large–small, and large–large interactions, respectively. The colloids are placed in a periodic cubic volume, with large-colloid volume fraction 5%. We take the particles masses to be m_0 , yielding a time scale $t_0 = \sigma_{LJ}\sqrt{m_0/\epsilon_{LJ}}$.

Surface bound charges are computed *in each time step* using the GMRES algorithm, which converges in 2 or 3 iterations for this system. The bound charge is discretized using 372 surface patches *per colloid*, placed on a shell of radius $3\sigma_{LJ}$, just below the excluded-volume radius $3.5\sigma_{LJ}$, resulting in more than 37 000 discrete charges in each system. This patch density yields a relative error of $\mathcal{O}(10^{-3})$ in the dielectric interaction energy of a large–small pair at contact. Starting from a random, nonoverlapping configuration, we investigate self-assembly by following the system for 1 000 000 time steps of $0.005t_0$, for a total duration of $5 000t_0$ per simulation run. The first 10% of each run is discarded. Temperature is controlled via a Langevin thermostat with a damping time of $20t_0$. To isolate electrostatic effects, we vary the *reduced* temperature $\tau = k_B T/U_{\text{coul}}$, where $U_{\text{coul}} = q^2/(4\pi\epsilon_0\kappa_m(4\sigma_{LJ}))$ is the Coulomb interaction of a large and a small colloid at contact. For simplicity, we maintain $\epsilon_{LJ} = k_B T$. Then, without loss of generality, we may reduce the five physical quantities (q , κ_m , κ_{small} , κ_{large} , and T) to just two parameters ($\tilde{\kappa} = \kappa_{\text{large}}/\kappa_m$ and τ).

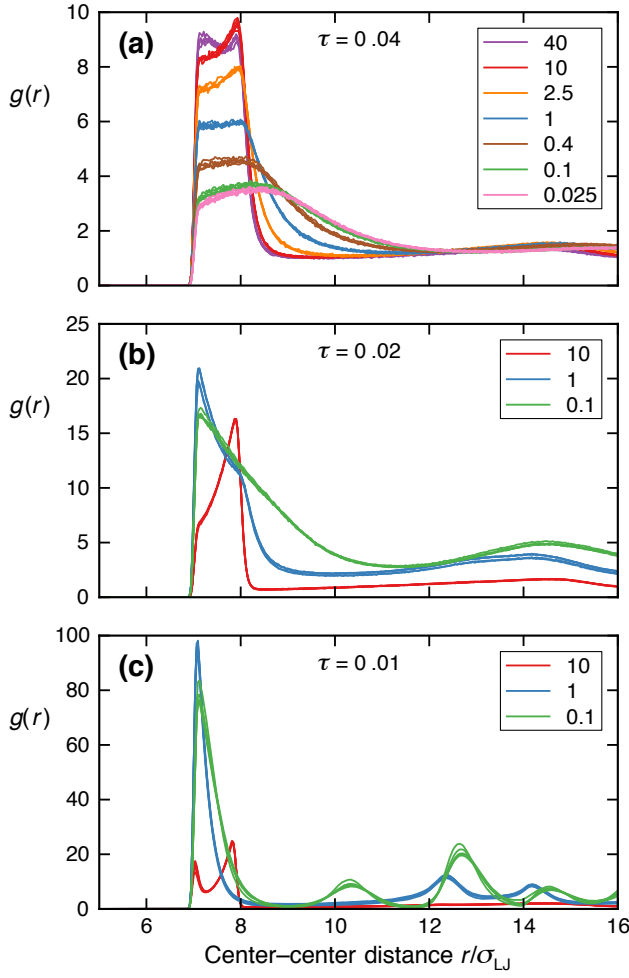


FIG. 2. Role of dielectric effects in size-asymmetric mixtures of charged, polarizable colloids at successively lower reduced temperatures (a) $\tau = 0.04$, (b) 0.02, (c) 0.01. Each panel shows the radial distribution function $g(r)$ of large colloids for different reduced dielectric constants $\tilde{\kappa}$. At high temperatures (panel (a)), the strongest binding occurs for $\tilde{\kappa} > 1$ as polarization charges enhance the large-small binding. Dielectric many-body effects reverse the situation at low temperatures (panel (c)), where $g(r)$ shows the most pronounced structure for $\tilde{\kappa} < 1$. To exclude equilibration artifacts, all runs are repeated five times from different initial conditions, with results that agree within statistical error.

As simulations are performed at successively lower temperatures, the colloids exhibit a strong tendency to aggregate, as shown by the large-particle radial distribution function in Figs. 2a–c. First, we consider $g(r)$ for the highest reduced temperature $\tau = 0.04$ (Fig. 2a). Here, the colloids are not strongly bound and $g(r)$ shows a broad peak from $r = 7\sigma_{LJ}$ (large particles in contact, typically bonded by two small colloids) to $r \approx 8\sigma_{LJ}$ (large colloids separated by a small colloid). Compared to non-polarizable colloids ($\tilde{\kappa} = 1$), colloids with higher dielectric constant than the solvent ($\tilde{\kappa} > 1$) exhibit a stronger peak, as the bound-charge interactions become attrac-

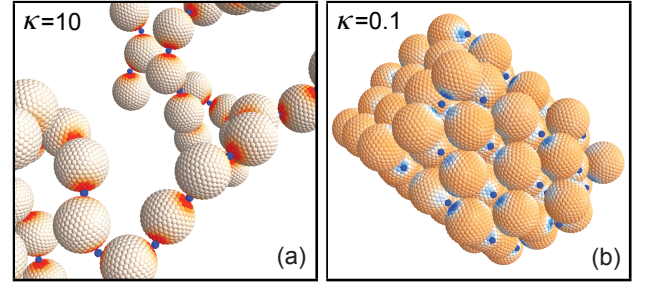


FIG. 3. Example of the importance of polarization charges in electrostatic self-assembly. Low-temperature equilibrium configurations of a size-asymmetric binary mixture of colloids at reduced dielectric constant (a) $\tilde{\kappa} = 10$ and (b) $\tilde{\kappa} = 0.1$. The large colloids carry a positive charge and the small colloids are negatively charged. The net surface charge density (bare and induced charges) is represented by red (positive) and blue (negative) color gradients. The string-like structures in panel (a) arise owing to the prominence of dielectric many-body effects (see text). The NaCl structure in panel (b) is consistent with the correlation function in Fig. 2c.

tive (Fig. 1) and the small colloids mediate an attractive effective interaction between the large ones. Conversely, for low-dielectric constant colloids ($\tilde{\kappa} < 1$) the polarization charges counteract the Coulombic large-small attraction, diminishing and broadening the primary peak in $g(r)$. The repulsive interaction between the polarization charges induced by a small colloid on surrounding colloids amplifies this effect. Thus, dielectric effects at this temperature can be qualitatively understood through decomposition into two-body interactions.

As the reduced temperature is lowered to $\tau = 0.02$ (Fig. 2b), the situation changes. In the absence of dielectric effects ($\tilde{\kappa} = 1$) the broad peak observed at $\tau = 0.04$ gives way to a prominent contact peak only, signaling the Coulombic binding of two large colloids by small colloids. For $\tilde{\kappa} = 0.1$ the repulsive polarization charges diminish the height of this peak somewhat. Most striking, however, is the situation at $\tilde{\kappa} = 10$, where a prominent peak at $r = 8\sigma_{LJ}$ arises; here *three-body* interactions qualitatively alter the situation, as the induced bound charges on the colloids simultaneously enhance the large-small attraction and yield an effective local repulsion between the large colloids.

Finally, at the lowest reduced temperature $\tau = 0.01$ (Fig. 2c), entropic effects become negligible. The pair correlation function reveals a complete reversal from the weakly bound system at $\tau = 0.04$, with the strongest binding and most ordered structure now occurring at the *lowest* $\tilde{\kappa}$. These findings are opposite of the expectations based upon two-body interactions and result from emergent dielectric many-body interactions. Indeed, the peaks in $g(r)$ at $\tilde{\kappa} = 10$, 1, and 0.1 correspond to three different structures: strings (Fig. 3a), hexagonally-packed “sheets” (not shown), and crystalline aggregates

with a sodium chloride structure (Fig. 3b), respectively. The string-like aggregates exhibit a particularly noteworthy example of many-body effects. Once two small colloids are bound to diametrically opposite locations on a large colloid (minimizing their mutual repulsion), the locally induced (positive) polarization charge in conjunction with the net-charge requirement Eq. (9) results in a negative polarization charge induced around the “equator,” hindering the association of additional small colloids with this large colloid and instead promoting the formation of string-like structures. Not only do such self-assembled chains offer a striking example of the qualitative changes that can be induced by polarization effects, but they may also provide a (partial) explanation of experimentally observed chain formation of nanoparticles (for which the many-body effects will be stronger than for larger colloids) in a range of solvents [34–36].

In conclusion, using a newly introduced efficient and generally applicable method [16] that permits simulations of a broad range of systems with fully resolved dielectric many-body effects, we have explored the role of these effects in the aggregation of colloids and nanoparticles. We demonstrated that polarization can qualitatively alter the self-assembled structures. Our approach, which immediately generalizes to arbitrarily complex dielectric geometries, provides insight into the underlying mechanisms of recent experimental observations and makes it possible to exploit dielectric effects to control colloidal self-assembly.

This material is based upon work supported by the National Science Foundation under Grant Nos. DMR-1006430 and DMR-1310211. We thank D. Sinkovits for useful discussions and acknowledge allocation of computing time on Northwestern University’s Quest cluster. K.B. acknowledges support from the Theoretical Division and CNLS at Los Alamos National Laboratory.

* Corresponding author: luijten@northwestern.edu

- [1] W. B. Russel, D. A. Saville, and W. R. Schowalter, *Colloidal Dispersions* (Cambridge University Press, Cambridge, U.K., 1989).
- [2] R. J. Hunter, *Foundations of Colloid Science*, 2nd ed. (Oxford University Press, Oxford, 2001).
- [3] M. E. Leunissen, C. G. Christova, A.-P. Hynninen, C. P. Royall, A. I. Campbell, A. Imhof, M. Dijkstra, R. van Roij, and A. van Blaaderen, *Nature* **437**, 235 (2005).
- [4] T. P. Doerr and Y.-K. Yu, *Phys. Rev. E* **73**, 061902 (2006).
- [5] D. G. Levitt, *Biophys. J.* **22**, 209 (1978).
- [6] M. Hoyles, S. Kuyucak, and S.-H. Chung, *Comp. Phys. Comm.* **115**, 45 (1998).
- [7] R. Allen, J.-P. Hansen, and S. Melchionna, *Phys. Chem. Chem. Phys.* **3**, 4177 (2001).
- [8] D. Boda, D. Gillespie, W. Nonner, D. Henderson, and B. Eisenberg, *Phys. Rev. E* **69**, 046702 (2004).
- [9] S. Tyagi, M. Süzen, M. Sega, M. Barbosa, S. S. Kantorovich, and C. Holm, *J. Chem. Phys.* **132**, 154112 (2010).
- [10] V. Jadhao, F. J. Solis, and M. Olvera de la Cruz, *Phys. Rev. Lett.* **109**, 223905 (2012).
- [11] T. Croxton, D. A. McQuarrie, G. N. Patey, G. M. Torrie, and J. P. Valteau, *Can. J. Chem.* **59**, 1998 (1981).
- [12] G. M. Torrie, J. P. Valteau, and G. N. Patey, *J. Chem. Phys.* **76**, 4615 (1982).
- [13] R. Kjellander and S. Marčelja, *J. Chem. Phys.* **82**, 2122 (1985).
- [14] R. Messina, *J. Chem. Phys.* **117**, 11062 (2002).
- [15] J. Reščič and P. Linse, *J. Chem. Phys.* **129**, 114505 (2008).
- [16] K. Barros, D. Sinkovits, and E. Luijten, *J. Chem. Phys.* **140**, 064903 (2014).
- [17] J. D. Jackson, *Classical Electrodynamics*, 3rd ed. (Wiley, New York, 1999).
- [18] J. N. Israelachvili, *Intermolecular and Surface Forces*, 3rd ed. (Academic, San Diego, 2011).
- [19] H. Hoshi, M. Sakurai, Y. Inoue, and R. Chûjô, *J. Chem. Phys.* **87**, 1107 (1987).
- [20] Y. Saad and M. H. Schultz, *SIAM J. Sci. Stat. Comput.* **7**, 856 (1986).
- [21] H. van der Vorst, *SIAM J. Sci. Stat. Comput.* **13**, 631 (1992).
- [22] L. Greengard and V. Rokhlin, *Acta Numerica* **6**, 229 (1997).
- [23] C. Sagui and T. Darden, *J. Chem. Phys.* **114**, 6578 (2001).
- [24] H. A. Pohl, *J. Appl. Phys.* **22**, 869 (1951).
- [25] T. B. Jones, *Electromechanics of particles* (Cambridge University Press, Cambridge, U.K., 1995).
- [26] J. M. Romero-Enrique, G. Orkoulas, A. Z. Panagiotopoulos, and M. E. Fisher, *Phys. Rev. Lett.* **85**, 4558 (2000).
- [27] J. Liu and E. Luijten, *Phys. Rev. Lett.* **93**, 247802 (2004).
- [28] S. R. Van Tomme, C. F. van Nostrum, M. Dijkstra, S. C. D. Smedt, and W. E. Hennink, *Eur. J. Pharm. Biopharm.* **70**, 522 (2008).
- [29] H.-Y. Kim, J. O. Sofo, D. Velegol, M. W. Cole, and A. A. Lucas, *J. Chem. Phys.* **124**, 074504 (2006).
- [30] M. W. Cole, L. N. Gergidis, J. P. McNutt, D. Velegol, H.-Y. Kim, and Z. K. Bond, *J. Nanophotonics* **4**, 041560 (2010).
- [31] B. W. Ninham and V. A. Parsegian, *J. Theor. Biol.* **31**, 405 (1971).
- [32] D. Y. C. Chan and D. J. Mitchell, *J. Colloid Interface Sci.* **95**, 193 (1983).
- [33] I. Popa, P. Sinha, M. Finessi, P. Maroni, G. Papastavrou, and M. Borkovec, *Phys. Rev. Lett.* **104**, 228301 (2010).
- [34] Z. Tang, N. A. Kotov, and M. Giersig, *Science* **297**, 237 (2002).
- [35] J. H. Liao, K. J. Chen, L. N. Xu, C. W. Ge, J. Wang, L. Huang, and N. Gu, *Appl. Phys. A* **76**, 541 (2003).
- [36] S. Lin, M. Li, E. Dujardin, C. Girard, and S. Mann, *Adv. Mater.* **17**, 2553 (2005).